Effect of Polymer Processing on the Performance of Poly(3-hexylthiophene)/ZnO Nanorod Photovoltaic Devices

ARTICLE *in* THE JOURNAL OF PHYSICAL CHEMISTRY C · OCTOBER 2007

Impact Factor: 4.77 · DOI: 10.1021/jp0757816

Article

Effect of Polymer Processing on the Performance of Poly(3-hexylthiophene)/ZnO Nanorod Photovoltaic Devices

Dana C. Olson, Yun-Ju Lee, Matthew S. White, Nikos Kopidakis, Sean E. Shaheen, David S. Ginley, James A. Voigt, and Julia W. P. Hsu

J. Phys. Chem. C, **2007**, 111 (44), 16640-16645 • DOI: 10.1021/jp0757816

Effect of Polymer Processing on the Performance of Poly(3-hexylthiophene)/ZnO Nanorod Photovoltaic Devices

Dana C. Olson,*,† Yun-Ju Lee,† Matthew S. White,‡ Nikos Kopidakis,‡ Sean E. Shaheen,‡ David S. Ginley,‡ James A. Voigt,† and Julia W. P. Hsu†

Sandia National Laboratories, Albuquerque, New Mexico 87185, and National Renewable Energy Laboratory, Golden, Colorado 80401

Received: July 23, 2007; In Final Form: August 23, 2007

Effective infiltration of the polymer into the nanostructured oxide is critical for optimizing the performance of hybrid π-conjugated polymer/nanostructured metal oxide semiconductor photovoltaic devices. We investigated the effect of polymer processing parameters, solvent selection, and thermal annealing on poly(3-hexylthiophene) (P3HT)/ZnO nanorod photovoltaic devices and found that these play an important role in the degree of polymer infiltration and the subsequent device performance. We demonstrate that using dichlorobenzene as a solvent produced better performance devices than using chloroform. In addition, the infiltration of P3HT into the ZnO nanorod array has been improved through annealing and subsequent slow cooling. Time-resolved microwave conductivity studies reveal an increase in the photoconductivity of the composite devices with annealing, resulting from changes in both the polymer and ZnO. The device performance was shown to increase with enhanced infiltration, and the devices that had been slow cooled from melt at 225 °C demonstrated a V_{OC} of 440 mV, a J_{SC} of 1.33 mA/cm^2, a fill factor of 48%, and a power conversion efficiency of 0.28%. In contrast to previously published results on P3HT infiltrated into mesoporous TiO_2 (*Appl. Phys. Lett.* **2003**, *83*, 3380), we found that the device performance improves with increasing amount of the polymer embedded in the ZnO arrays, through proper solvent selection and polymer processing.

Introduction

Organic photovoltaic (OPV) devices based on nanostructured composites of electron donor and acceptor materials promise to deliver future solutions to the low-cost energy generation.[2] Bulk heterojunction devices based on polymer−fullerene blends already demonstrate power conversion efficiencies exceeding 5%.[3−8] Such devices can be printed using roll-to-roll compatible techniques while maintaining high efficiencies.[9,10] However, the control of the blend morphology is determined by the solvent selection and annealing processes that must be optimized for each donor−acceptor combination.[5,7,8] Other electron acceptor materials have been investigated in hopes of improving charge transport. Bulk heterojunction devices made of polymer−metal oxide nanoparticle blends have been shown to be reasonably efficient.[11−13] However, the morphology of the composite system can be more deliberately controlled by employing nanoporous metal oxide acceptors that are deposited directly on the substrate and subsequently filled with a conjugated polymer donor.[14,15] In addition to the improved electron mobility associated with ordered metal oxide nanostructures, the hole mobility of the conjugated polymer could be enhanced in the direction normal to the substrate by infiltrating the polymer into a nanoporous metal oxide film with vertically oriented pores, due to an alignment of the polymer chains along the walls of the pores.[16] Arrays of zinc oxide (ZnO) nanorods are particularly well suited for this application as they can be grown normal to the substrate using low-temperature hydrothermal growth, have excellent electron mobilities, and have a rod-to-rod spacing that is compatible with the short exciton diffusion lengths (<10 nm) found in conjugated polymer donor materials.[17−19] Results on hybrid polymer−ZnO nanorod composite devices have yet to demonstrate increased performance over blend devices,[20−23] in part due to the lack of optimized device structures and processing.

The infiltration of the polymer into the nanostructured metal oxide is of particular importance for optimizing the performance of these hybrid devices with small rod-to-rod spacings. Previous studies on polymer/ZnO nanorod composites have employed ZnO arrays with large pore sizes (~100 nm) due to the disordered orientation of the nanorods.[20,22,23] As such, these devices have not employed extensive infiltration methods beyond spin coating the polymer on the ZnO nanorod arrays. In a previous publication, we have demonstrated excellent control in the synthesis of ordered ZnO nanorod arrays, resulting in less than 20 nm spacing between the rods.[24] Such arrays should provide a near ideal architecture for an ordered organic−inorganic based bulk heterojunction device.[14,15] The purpose of this paper is to investigate how different poly(3-hexylthiophene) (P3HT) infiltration techniques affect the performance of solar cell devices based on these densely ordered ZnO nanorod arrays. In particular, we report the effects of solvent selection and annealing conditions on the performance of these solar cell devices.

Materials and Methods

Sample Preparation. Devices were fabricated on patterned indium tin oxide (ITO) coated glass substrates. The sheet resistance of the ITO was 13 Ω/cm^2 (Colorado Concept Coatings

* To whom correspondence should be addressed. E-mail: dolson@sandia.gov.
† Sandia National Laboratories.
‡ National Renewable Energy Laboratory.

10.1021/jp0757816 CCC: $37.00
Published on Web 10/05/2007

LLC). The 1 in. × 1 in. substrates were cleaned by ultrasonic agitation in dichloromethane (10 min) and acetone (10 min), rinsing with methanol, and then exposing to an UV-ozone treatment (UVO-Cleaner, Jelight) for 20 min. A ZnO seed layer was deposited from a 5 mM solution of zinc acetate dihydrate (Aldrich) in ethanol and annealed at 350 °C for 20 min to form a ZnO film as described previously.[24,25] ZnO nanorods were subsequently grown from the seeded substrate placed face down in 24 mL of a solution containing 25 mM zinc nitrate (Aldrich) and 25 mM hexamethylenetetramine (HMT) at 92.5 °C for 75 min. The samples were then rinsed with DI water and dried in air. The resulting ZnO nanorods were ~200 nm in length and ~45 nm in diameter. By varying the growth time, nanorods of different lengths can be grown. Planar ZnO films were also fabricated by spin coating at 2000 rpm from a 0.75 M zinc acetate dihydrate in 2-methoxyethanol with a 1:1 ratio of zinc acetate to ethanol amine. The sol−gel film was subsequently annealed on a hot plate in air at 300 °C for 10 min, after which the film was rinsed with DI water, acetone, and isopropanol. According to X-ray diffraction measurements, the ZnO nanorod arrays were very well oriented with the (0001) direction normal to the substrate. The sol−gel ZnO films were polycrystalline, but highly (0001) textured.

Poly(3-hexylthiophene) (P3HT) was used as purchased from Rieke Metals. Prior to depositing the P3HT, the ZnO films were heated on a hot plate at 150 °C in air for 30 min followed by cooling under flowing N_2. Immediately after this process, the samples were placed on the spin coater and the P3HT films were deposited. Films were spin coated from solutions of P3HT either dissolved in chloroform (20 g/L) at a spin speed of 800 rpm or dissolved in 1,2-dichlorobenzene (40 g/L) at a spin speed of 600 rpm, both for 60 s. The samples spin coated from dichlorobenzene were then placed in covered glass Petri dishes and allowed to dry over the course of 45 min. The dry samples were then used as deposited or were subsequently annealed at 150 and 225 °C in a nitrogen atmosphere to enhance polymer infiltration. The annealing time at 150 °C was 10 min. When heated to 225 °C, the polymer melted and then was allowed to cool slowly for ~45 min to help recrystallize the polymer. Finally, the silver electrodes were thermally evaporated at a pressure of 8×10^{-7} Torr with a total thickness of 100 nm. The resulting device area was 0.1 cm^2.

Sample Characterization. UV−vis absorption spectra were measured using an USB 2000 spectrometer (Ocean Optics, Inc.) equipped with a USB-ISS-UV-VIS sampling system . X-ray diffraction data were collected on a Bruker D-8 instrument. The morphology of the ZnO nanorods and the P3HT/ZnO nanorod composites was characterized using a Zeiss field-emission source scanning electron microscope (SEM). The samples were prepared for cross-sectional SEM by scoring the substrate, cooling them in liquid nitrogen, and cleaving the cold substrates to obtain a clear cross-section. The current density−voltage ($J-V$) response of the devices was measured with a Keithley 238 high current source power meter on a Spectrolab XT-10 solar simulator, which was calibrated for AM1.5 illumination with a light intensity of 100 mW/cm^2 using a reference Si solar cell. The external quantum efficiency (EQE) spectra were measured using a calibrated Si photodiode with a spot size smaller than the device area and with an intensity of 2 μW at 520 nm. The photoconductivities of the polymer, nanorods, and composites were measured using the contactless time-resolved microwave conductivity (TRMC) technique as described previously.[18,26,27] In brief, the change in the microwave power absorbed by the sample can be directly related to the photoinduced conductance, ΔG, of the films by $\Delta P/P = -K\Delta G$, where K is an experimentally determined calibration factor derived from the resonance characteristics of the cavity and the dielectric properties of the samples used. Since charge carriers will be generated during the pulse and eventually will decay, ΔG will be time dependent and referred to as "photoconductance transient". The instrument response is ~10 ns, which is limited by the response time of the microwave cavity. The end-of-pulse photoconductance, ΔG_{EOP}, is related to the product of the quantum yield for the mobile charge carrier generation per absorbed photon under our 5 ns long pulses (ϕ) and the sum of their mobilities ($\Sigma\mu$) by $\varphi\Sigma\mu = \Delta G_{EOP}/I_0 F_A \beta q_e$, where I_0 is the incident photon flux, F_A is the fraction of incident light absorbed by the film, β is the ratio between the broad and narrow inner dimensions of the waveguide used (2.08 in this case), and q_e is the elementary charge.[18,26−28] For the TRMC measurements on P3HT or P3HT/ZnO nanorod composites, the polymer was pumped with 500 nm laser pulses, while the measurements on the ZnO nanorods were carried out under excitation with 300 nm pulses.

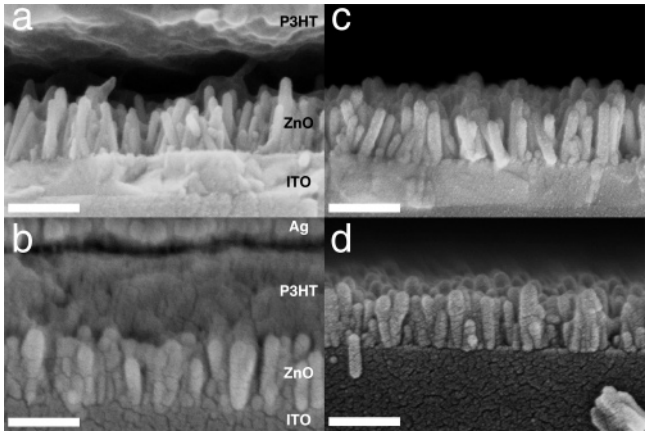

Figure 1. Cross-sectional SEM images of P3HT/ZnO nanorod composite PV devices with P3HT spin coated from chloroform (a) and with P3HT spin coated from 1,2-dichlorobenzene (b). Also shown are images after removing the polymer on top of the rods: chloroform spin coated (c); 1,2-dichlorobenze spin coated (d). Scale bars: 200 nm.

Results and Discussion

Past studies on P3HT/ZnO-based devices have relied on polymer films spin coated from chloroform or chlorobenzene on disordered ZnO nanorod arrays.[20,22,23] Here we first examine the choice of the solvent on the infiltration of P3HT into dense, ordered ZnO nanorod arrays. Figure 1 shows the dramatic effect of the solvent selection. When the P3HT films are spin coated from chloroform on top of the ordered ZnO nanorod arrays, there is very poor infiltration of the polymer into the pore structure of the ZnO arrays, as seen in Figure 1a. Clearly, the wetting of the ZnO structures by the P3HT is poor, resulting in a void space on top of the ZnO rods. It has been reported that increased film drying time can enhance the molecular ordering and, therefore, the carrier mobility in P3HT/fullerene blends.[5,29] In these blends, films spin coated from dichlorobenzene were allowed to dry in covered Petri dishes over the course of 20 min. Here, we have employed the solvent annealing process through the use of dichlorobenzene, a high boiling point and low vapor pressure solvent, to more effectively infiltrate P3HT into ZnO nanorod arrays. Figure 1b shows that the infiltration of the P3HT spin coated from dichlorobenzene is greatly enhanced. To gauge the amount of polymer that was effectively infiltrated into the small pores in the ZnO nanorod array, we removed any polymer not infiltrated by soaking the composites

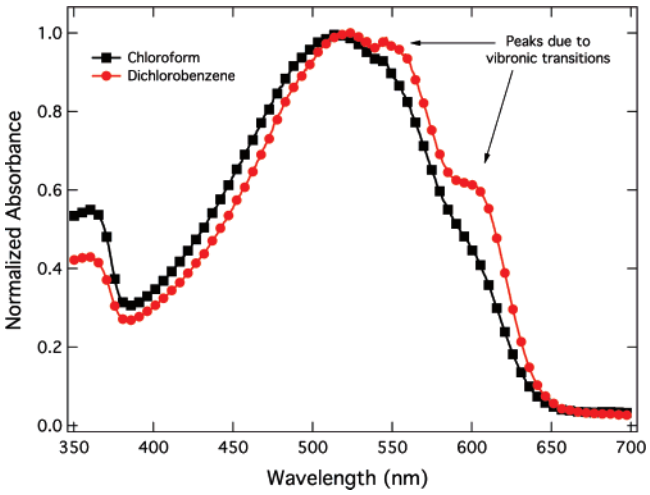

Figure 2. Normalized absorbance spectra for P3HT/ZnO nanorod composites with P3HT spin coated from chloroform (black squares) and with P3HT spin coated from 1,2-dichlorobenzene (red circles).

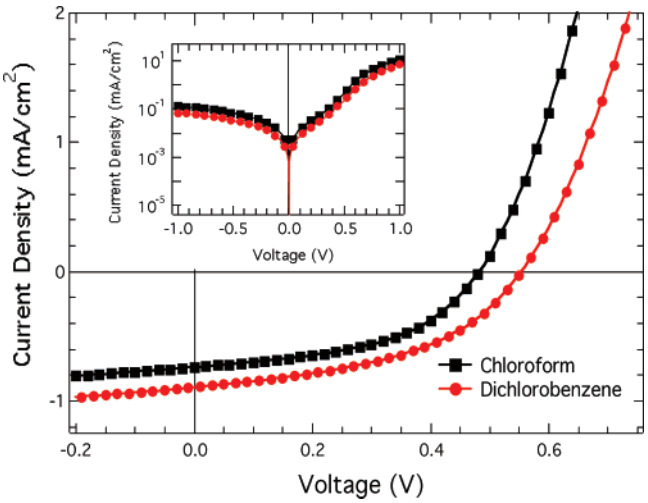

Figure 3. Current density vs voltage ($J-V$) for illuminated (at AM1.5) ITO/ZnO nanorod/P3HT/Ag devices with P3HT spin coated from chloroform (black squares) and with P3HT spin coated from 1,2-dichlorobenzene (red circles). The inset shows the dark $J-V$ characteristics of the two devices.

in chloroform for 10 s and rinsing with more chloroform.[30] The polymer not infiltrated dissolved immediately, and the infiltrated polymer remained in the pores even after long exposures (~5 min) or multiple soak/rinse cycles. The optical density increased from 0.1 to 0.15 when changing solvents from chloroform to dichlorobenzene. Cross-sectional SEM images of the rinsed devices are presented in Figure 1c,d. Figure 2 compares the optical absorption spectra for P3HT/ZnO nanorod composites with P3HT spin coated from chloroform and dichlorobenzene. The shoulders due to vibronic transitions in the UV−vis spectra of the dichlorobenzene films were enhanced, as interpreted by the increased shoulders at 550 and 600 nm. Previous thin film transistor work has shown that the presence of these shoulders correlates to enhanced hole mobility in the polymer.[31−33] Thus, the increased molecular order observed in blend devices prepared from dichlorobenzene solutions was also observed in these P3HT/ZnO nanorod composites.

As seen in Figure 1a, the P3HT forms a large gap with the top, polar (0001) surfaces of ZnO nanorods and wicks in among the nonpolar ($10\bar{1}0$) surfaces.[34,35] The polarity of ZnO surfaces might be an additional complication to the polymer infiltration. In previous ZnO nanorod/P3HT solar cell work, disordered and less dense ZnO nanorod arrays were used, which present the polymer with more of the nonpolar surfaces of the ZnO nanorods and may help polymer intercalation through more favorable interfacial interactions. In this work, where well-oriented (vertical) ZnO nanorod arrays were used, the P3HT largely was exposed to the top, polar surface of the ZnO, which might serve as a barrier to efficient polymer infiltration.

Figure 3 shows that the photovoltaic response of the dichlorobenzene devices is greatly enhanced. When switching from chloroform to dichlorobenzene, the open circuit voltage (V_{OC}) increased from 484 to 556 mV, the short circuit current density (J_{SC}) increased from 0.74 to 0.90 mA/cm^2, and the power conversion efficiency (η) increased from 0.17 to 0.23%, as seen in Table 1. This is believed to be due to the increased infiltration of the polymer into the ZnO nanorod structures as well as due to enhanced carrier transport through the more ordered polymer phase. Therefore, the solvent selection and drying time (solvent annealing) have a dramatic effect on polymer infiltration, ordering, and consequently on the as-prepared P3HT/ZnO nanorod composite solar cell performance.

To further enhance the polymer infiltration and device performance, the effect of annealing of the P3HT/ZnO composites was studied. Following published work on the melt infiltration of P3HT into mesoporous TiO_2 films with pore diameters of 6 nm,[1,30] we have employed a similar approach to facilitate the infiltration of the P3HT into the ordered ZnO nanorod arrays in this study. The P3HT films were spin coated from dichlorobenzene onto ZnO nanorods. Figure 4a−c shows cross-sectional SEM images of ZnO/P3HT photovoltaic devices with as-made P3HT films (a) and those annealed at 150 °C (b) and 225 °C (c) under nitrogen. It is evident that the infiltration of the polymer enhanced with increasing anneal temperature. It is important to note that the apparent loss in adhesion between Ag and P3HT in the sample annealed at 225 °C (Figure 4c) is caused by the freeze-fracture process used to prepare cross-sectional specimens. The amount of infiltrated polymer can be estimated by optical absorption after rinsing the samples with chloroform to remove the uninfiltrated polymer on top of the rod arrays.[30] It is clear from cross-sectional SEM images (Figure 4d−f) that more of the P3HT adhered to the ZnO nanorods in the annealed samples. The optical density of the embedded P3HT increased from 0.15 to 0.25 after annealing at 150 °C and to 0.95 after melt infiltration at 225 °C.

TABLE 1: Photovoltaic Properties of Devices[a] Spin Coated from Chloroform (CF) and 1,2-Dichlorobenzene (DCB)

solvent	temperature (°C)	V_{OC} (mV)	J_{SC} (mA/cm^2)	FF (%)	η (%)
CF	NA	484	0.74	48.5	0.17
DCB	NA	556	0.90	45.8	0.23
DCB	150	438	1.24	46.6	0.25
DCB	225	443	1.33	48.4	0.28

[a] Devices were annealed at the temperature or were not annealed (NA) as indicated.

Figure 5 shows the best results we have obtained on P3HT/ZnO nanorod composite solar cells for each polymer annealing condition outlined above. The photovoltaic performance of the annealed P3HT/ZnO nanorod composites increased with annealing temperature, mainly due to the larger J_{SC}. The J_{SC} increased from 0.90 mA/cm^2 when not annealed to 1.24 mA/cm^2 after annealing at 150 °C and to 1.33 mA/cm^2 after annealing at 225 °C, as seen in Table 1. This increase in J_{SC} with annealing appears to correlate well with the enhancement in P3HT infiltration as discussed above. Improved polymer infiltration into the ZnO nanorod array increased the interfacial area of the device, leading to more efficient charge collection

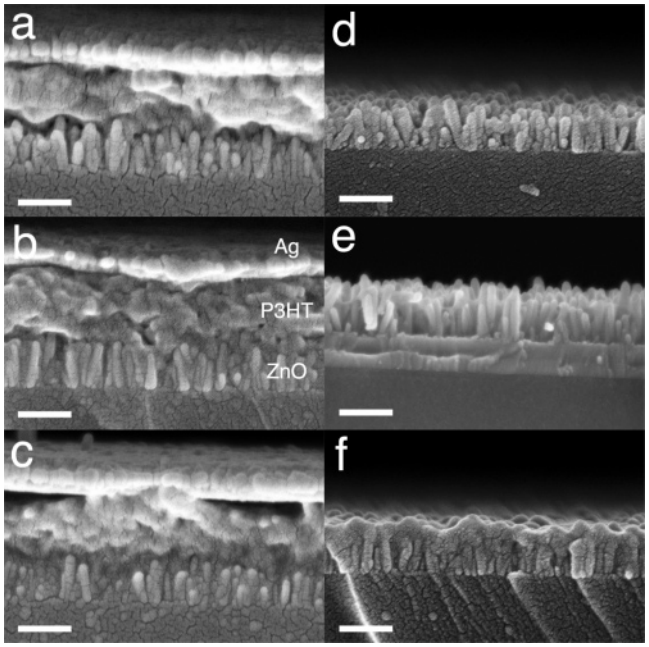

Figure 4. Cross-sectional SEM images of P3HT/ZnO nanorod composite PV devices: without annealing (a); with annealing at 150 °C (b); with annealing at 225 °C (c). Also shown are images after removing the polymer on top of the rods: no anneal (d); annealing at 150 °C (e); annealing at 225 °C (f). Scale bars: 200 nm.

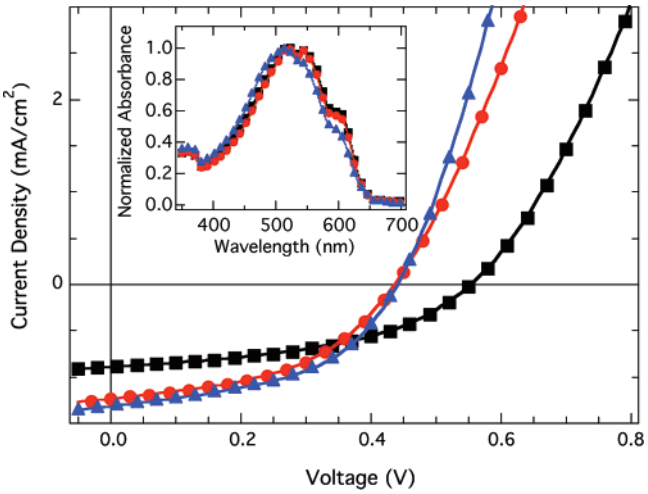

Figure 5. Best photovoltaic performance (illuminated at AM1.5) for ITO/ZnO nanorod/P3HT/Ag devices: not annealed (black squares); annealed at 150 °C (red circles); annealed at 225 °C (blue triangles). The inset shows normalized absorbance spectra of P3HT/ZnO nanorod devices: not annealed (black squares); annealed at 150 °C (red circles); annealed at 225 °C (blue triangles).

from the device. As a result the power conversion efficiency (η) increased from 0.23% without annealing to 0.25% after annealing at 150 °C and to 0.28% after annealing at 225 °C. While the devices presented here showed that the V_{OC} decreased from over 550 to 440 mV after annealing at 150 or 225 °C, this trend is not consistently observed. Currently, the variation in the V_{OC} is not yet fully understood and will be the subject of further investigation.

We observed through optical absorption data that when neat films of P3HT were cooled after melting (225 °C anneal), the polymer chains became more disordered than those of as-prepared neat films made by slow drying from dichlorobenzene. This can be identified through loss of the shoulders due to vibronic transitions in the spectra at 550 and 600 nm. Therefore,

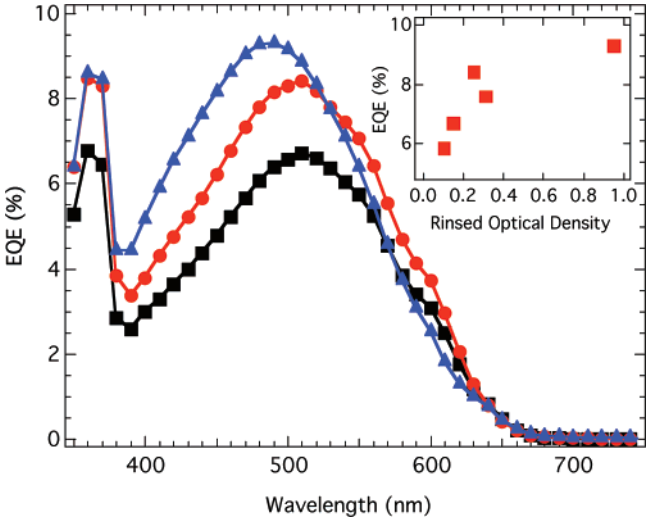

Figure 6. External quantum efficiency spectra of ITO/ZnO nanrod/P3HT/Ag devices: not annealed (black squares); annealed at 150 °C (red circles); annealed at 225 °C (blue triangles). The inset shows EQE vs rinsed optical density of P3HT/ZnO rod composite devices.

to minimize the loss of molecular ordering when the P3HT in the ZnO nanorod device was heated at 225 °C, it was allowed to cool from the melt slowly over the course of 45 min in order to imitate the organization of the polymer chains when the films were dried slowly after being spun from dichlorobenzene. Though slow cooling increases the order in melt-processed films, we still observed a small loss in the polymer chain ordering after cooling slowly from the melt (Figure 5 inset). Additionally, the melt processing erases the processing history, so that melt infiltrated films prepared from dichlorobenzene are identical to those made from chloroform.

The improvement in device performance with annealing is also reflected in the external quantum efficiency (EQE) of the devices, as seen in Figure 6. Here, we observed the same trend of increased photon to current conversion efficiency as a result of increased annealing temperature. Additionally, there was a small blue shift in the spectrum when the polymer was annealed at 225 °C, which was also observed through the loss of shoulders in the absorbance spectrum of the device (Figure 5 inset). This leads to a decreased overlap with the solar spectrum as well as a reduced hole mobility, which would reduce the J_{SC} from what would be expected due to the enhanced polymer infiltration after annealing at 225 °C. Despite this, the device annealed at 225 °C demonstrated a higher J_{SC} than the other devices. This result points to a significant improvement in the infiltration of the P3HT or better electrical contact between P3HT and ZnO.

Previous work on the P3HT/mesoporous TiO_2 composites has demonstrated that the transport properties of the polymer were substantially diminished after melt infiltration.[1] In that work, when the optical density of the embedded polymer was increased, the device EQE was reduced. This was attributed to a filtering effect of the polymer infiltrated deepest into the porous TiO_2 structure, where the hole mobility of the polymer was too low to allow for efficient carrier transport from this region upon photoexcitation. Hence, the absorption of light by the deeply infiltrated polymer led to a reduction in the amount of light available for the active region of the device, which was closer to the hole-collecting electrode, without contributing to photocurrent. In contrast, the annealing results in our P3HT/ZnO nanorod composites show the opposite trend; the EQE, J_{SC}, and device efficiency all increase with increasing polymer infiltration. The inset in Figure 6 demonstrates that the EQE

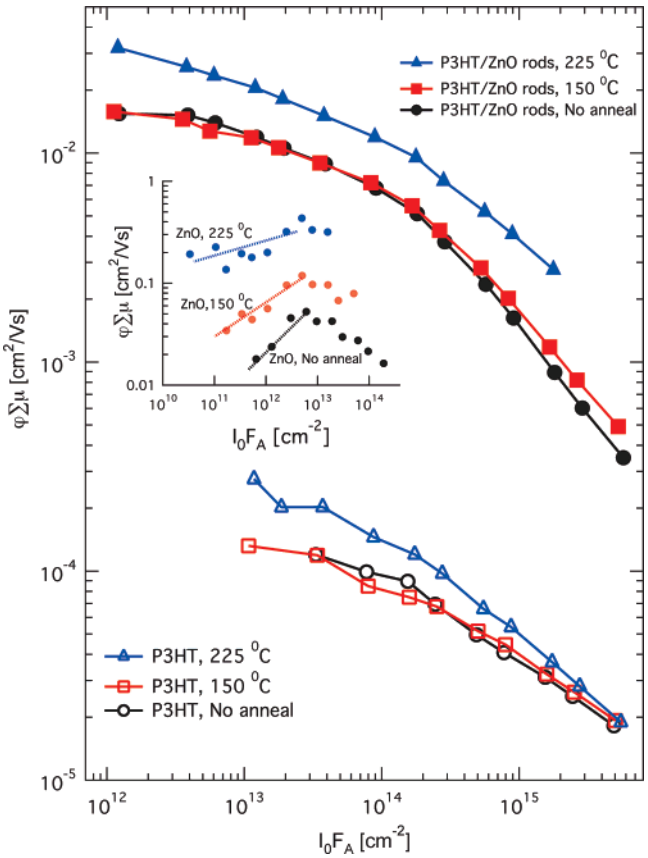

Figure 7. Photoconductivity per absorbed photon vs absorbed photon flux measured with TRMC under excitation with 500 nm pulses for P3HT (open symbols) and P3HT/ZnO rod composites (solid symbols): not annealed (black circles); annealed at 150 °C (red squares); annealed at 225 °C (blue triangles). The inset shows photoconductivity per absorbed photon versus absorbed photon flux measured with TRMC under excitation with 300 nm pulses for the ZnO nanorods: before annealing (black); annealed at 150 °C (red); annealed 225 °C (blue). The lines are guides to the eyes (see text).

increases with the amount of polymer infiltrated into the ZnO nanorod composite. These are data collected from a series of devices annealed at different infiltration temperatures as well as with devices based on 100 nm ZnO rods. The filtering effect is not observed, and hole transport is not the primary limiting factor of the performance of P3HT/ZnO nanorod devices. The difference in the two systems is likely due to the size and ordering of the pores. The ordered ZnO nanorod arrays have a larger pore size of ~20 nm compared to the 6 nm pore size in the mesoporous TiO_2. In addition, the pores in the ZnO nanorod arrays used in this study are vertically aligned, which might help to reduce the amount of disorder that is induced in the P3HT by infiltration into the mesoporous TiO_2. This, in turn, might help to preserve the intrinsic P3HT hole mobility and transport properties.

The effect of annealing was also investigated using TRMC. A comparison of the TRMC signal from the P3HT/ZnO nanorod and from P3HT only on glass is shown in Figure 7. The magnitude of the signal from the pure polymer that was not annealed is in good agreement with previous work.[27,28] In these films, which were spin coated from dichlorobenzene, we observed an increase in the TRMC signal only after melting at 225 °C. This could be attributed to a higher carrier generation yield in the bulk of the polymer,[27] which could compensate for a decreased hole mobility that would result from the polymer becoming less ordered as observed in the UV−vis spectra (Figure 5 inset).

While the signal from pure P3HT is dominated by the hole density and mobility,[28] the signal from the P3HT/ZnO samples is dominated by the electron density and mobility in ZnO.[27,36] The magnitude of the TRMC signal for the P3HT/ZnO nanorod sample is higher than what has been reported previously for the P3HT/ZnO nanoparticle blends[36] and the P3HT/ZnO bilayers.[27] The difference is attributed to the higher mobility in the ZnO nanorods compared to nanoparticles[37] and, in the case of the P3HT/ZnO bilayers,[27] to the increased surface area of the ZnO nanorod film. A similar trend with regard to P3HT annealing was observed in the P3HT/ZnO nanorod composites, which might suggest that the same changes in P3HT after melting contributed to the increased TRMC signal observed in the composites.

In order to investigate the changes in the transport properties of the rods themselves with annealing, we carried out TRMC measurements of the rods without a polymer under excitation with 300 nm laser pulses. The results are shown in Figure 7 (inset). The light intensity dependence of the TRMC signal for the nonannealed ZnO nanorod sample resembles that for TiO_2 nanoparticles.[26] At low light intensities, a trap-filling regime is observed (highlighted with the dotted line). With annealing, the TRMC signal increases and exhibits a weaker dependence on light intensity in the trapping regime. These observations indicate that annealing removes traps from the ZnO nanorods, in much the same way that the background illumination inactivates the traps in TiO_2.[26] While it is not possible to extract the exact dependence of the mobility of electrons in the ZnO rods on annealing temperature, the data indicate that the mobility increases with annealing, consistent with previous reports.[37]

In a previous paper, we showed that the photoconductivity of P3HT/$Zn_{1-x}Mg_xO$ correlates well with the electron mobility in the oxide layer, which is not observed here.[27] In particular, the results of P3HT/ZnO nanorod composites are the same without annealing and after annealing at 150 °C, while the bare ZnO nanorods show a ~2 fold increase in photoconductivity with the 150 °C annealing. In the P3HT/$Zn_{1-x}Mg_xO$ work, the only parameter that changed between samples was the electron mobility in the oxide caused by Mg alloying. However, in the present system annealing could cause multiple changes in the composite: the mobility of electrons in ZnO, the structure and transport properties of the polymer, and the surface area of contact between the oxide and the polymer. For example, the increase in the surface area and electron mobility in the ZnO with 225 °C annealing are expected to have a beneficial effect on the photoconductivity, but the annealing step could have a negative effect of decreasing the carrier mobility in the polymer, thereby partially reducing the expected overall increase. In addition, the increase in the ZnO electron mobility might be different in composites where the ZnO is capped with the P3HT in bare nanorod arrays. Therefore, it is currently not definitive to identify the primary cause of the increase in photoconductivity of the composite annealed at 225 °C.

Conclusions

In conclusion, we have demonstrated that polymer processing has a strong effect on P3HT/ZnO nanorod photovoltaic device performance. We showed that using dichlorobenzene as the solvent in place of chloroform led to enhanced infiltration, polymer order, and device performance in as-prepared devices. In addition, the infiltration of the P3HT into the ZnO nanorod array and device characteristics were both improved through annealing. Melting P3HT at 225 °C also increased the TRMC signal in the composite films, where the signal in both the

individual materials increased as well. The device performance was shown to increase with enhanced infiltration, and the devices that had been slow cooled from the melt at 225 °C have demonstrated a power conversion efficiency of 0.28%, a V_{OC} of 440 mV, a J_{SC} of 1.33 mA/cm^2, and a fill factor of 48%. In contrast to previously published results on P3HT infiltrated into mesoporous TiO_2, we found that EQE increases with increasing amount of polymer embedded in the ZnO nanorod arrays. The difference in the two systems can be attributed to the larger pore size and the vertical order in the ZnO nanorod arrays. Thus, these data clearly show that the optimization of solvent selection and polymer processing can significantly improve the performance of P3HT/ZnO nanorod composite devices.

Acknowledgment. The authors would like to thank Bonnie Mckenzie for SEM imaging and Nolanne Chang and Erik Spoerke for their initial investigation on P3HT infiltration. We acknowledge the IC Postdoctoral Fellowship Program, the Sandia LDRD program, and the NREL LDRD program for funding this research. Sandia is a multiprogram laboratory operated by Sandia Corporation, a Lockheed Martin Company, for the United States Department of Energy's National Nuclear Security Administration under contract DE-AC04-94AL85000.

References and Notes

(1) Coakley, K. M.; McGehee, M. D. *Appl. Phys. Lett.* **2003**, *83*, 3380.
(2) Shaheen, S. E.; Ginley, D. S.; Jabbour, G. E. *MRS Bull.* **2005**, *30*, 10.
(3) Brabec, C. J.; Hauch, J.; Choulis, S.; Schilinsky, P.; Zeira, E.; Sokolik, I. Challenges in Flexible Organic Phovoltaics. In *Organic and Nanoparticle Hybrid Photovoltaic Devices, MRS Spring Meeting*; Materials Research Society: San Francisco, 2007.
(4) Kim, Y.; Cook, S.; Tuladhar, S. M.; Choulis, S. A.; Nelson, J.; Durrant, J. R.; Bradley, D. D. C.; Giles, M.; McCulloch, I.; Ha, C.-S.; Ree, M. *Nat. Mater.* **2006**, *5*, 197.
(5) Li, G.; Shrotriya, V.; Huang, J.; Yao, Y.; Moriarty, T.; Emery, K.; Yang, Y. *Nat. Mater.* **2005**, *4*, 864.
(6) Ma, W.; Yang, C.; Gong, X.; Lee, K.; Heeger, A. J. *Adv. Funct. Mater.* **2005**, *15*, 1617.
(7) Padinger, F.; Rittberger, R. S.; Sariciftci, N. S. *Adv. Funct. Mater.* **2003**, *13*, 85.
(8) Shaheen, S. E.; Brabec, C. J.; Sariciftci, N. S.; Padinger, F.; Fromherz, T.; Hummelen, J. C. *Appl. Phys. Lett.* **2001**, *78*, 841.
(9) Schilinsky, P.; Waldauf, C.; Brabec, C. J. *Adv. Funct. Mater.* **2006**, *16*, 1669.
(10) Shaheen, S. E.; Radspinner, R.; Peyghambarian, N.; Jabbour, G. E. *Appl. Phys. Lett.* **2001**, *79*, 2996.
(11) Beek, W. J. E.; Wienk, M. M.; Janssen, R. A. J. *Adv. Mater.* **2004**, *16*, 1009.
(12) Beek, W. J. E.; Wienk, M. M.; Janssen, R. A. J. *Adv. Funct. Mater.* **2006**, *16*, 1112.
(13) Beek, W. J. E.; Wienk, M. M.; Kemerink, M.; Yang, X.; Janssen, R. A. J. *J. Phys. Chem. B* **2005**, *109*, 9505.
(14) Coakley, K. M.; Liu, Y.; Goh, C.; McGehee, M. D. *MRS Bull.* **2005**, *30*, 37.
(15) Coakley, K. M.; McGehee, M. D. *Chem. Mater.* **2004**, *16*, 4533.
(16) Coakley, K. M.; Srinivasan, B. S.; Ziebarth, J. M.; Goh, C.; Liu, Y.; McGehee, M. D. *Adv. Funct. Mater.* **2005**, *15*, 1927.
(17) Halls, J. J. M.; Pichler, K.; Friend, R. H.; Moratti, S. C.; Holmes, A. B. *Appl. Phys. Lett.* **1996**, *68*, 3120.
(18) Kroeze, J. E.; Savenije, T. J.; Vermeulen, M. J. W.; Warman, J. M. *J. Phys. Chem. B* **2003**, *107*, 7696.
(19) Lewis, A. J.; Ruseckas, A.; Gaudin, O. P. M.; Webster, G. R.; Burn, P. L.; Samuel, I. D. W. *Org. Electron.* **2006**, *7*, 452.
(20) Olson, D. C.; Piris, J.; Collins, R. T.; Shaheen, S. E.; Ginley, D. S. *Thin Solid Films* **2006**, *496*, 26.
(21) Olson, D. C.; Shaheen, S. E.; Collins, R. T.; Ginley, D. S. *J. Phys. Chem. C*, in press.
(22) Peiró, A. M.; Ravirajan, P.; Govender, K.; Boyle, D. S.; O'Brien, P.; Bradley, D. D. C.; Nelson, J.; Durrant, J. R. *J. Mater. Chem.* **2006**, *16*, 2088.
(23) Ravirajan, P.; Peiro, A. M.; Nazeeruddin, M. K.; Graetzel, M.; Bradley, D. D. C.; Durrant, J. R.; Nelson, J. *J. Phys. Chem. B* **2006**, *110*, 7635.
(24) Lee, Y.-J.; Sounart, T. L.; Scrymgeour, D. A.; Voigt, J. A.; Hsu, J. W. P. *J. Cryst. Growth* **2007**, *304*, 80.
(25) Greene, L. E.; Law, M.; Tan, D. H.; Montano, M.; Goldberger, J.; Somorjai, G.; Yang, P. *Nano Lett.* **2005**, *5*, 1231.
(26) Kroeze, J. E.; Savenije, T. J.; Warman, J. M. *J. Am. Chem. Soc.* **2004**, *126*, 7608.
(27) Piris, J.; Kopidakis, N.; Olson, D. C.; Shaheen, S. E.; Ginley, D. S.; Rumbles, G. *Adv. Funct. Mater.*, in press.
(28) Dicker, G.; Haas, M. P.; Siebbeles, L. D. A.; Warman, J. M. *Phys. Rev. B* **2004**, *70*, 045203.
(29) Li, G.; Yao, Y.; Yang, H.; Shrotriya, V.; Yang, G.; Yang, Y. *Adv. Funct. Mater.* **2007**, *17*, 1636.
(30) Coakley, K. M.; Liu, Y.; McGehee, M. D.; Frindell, K. L.; Stucky, G. D. *Adv. Funct. Mater.* **2003**, *13*, 301.
(31) Wang, G.; Swensen, J.; Moses, D.; Heeger, A. J. *J. Appl. Phys.* **2003**, *93*, 6137.
(32) Cho, S.; Lee, K.; Yuen, J.; Wang, G.; Moses, D.; Heeger, A. J.; Surin, M.; Lazzaroni, R. *J. Appl. Phys.* **2006**, *100*, 114503.
(33) Bao, Z.; Dodabalapur, A.; Lovinger, A. J. *Appl. Phys. Lett.* **1996**, *69*, 4108.
(34) Govender, K.; Boyle, D. S.; Kenway, P. B.; O'Brien, P. *J. Mater. Chem.* **2004**, *14*, 2575.
(35) Peterson, R. B.; Fields, C. L.; Gregg, B. *Langmuir* **2004**, *20*, 5114.
(36) Quist, P. A. C.; Beek, W. J. E.; Wienk, M. M.; Janssen, R. A. J.; Savenije, T. J.; Siebbeles, L. D. A. *J. Phys. Chem. B* **2006**, *110*, 10315.
(37) Baxter, J. B.; Schmuttenmaer, C. A. *J. Phys. Chem. B* **2006**, *110*, 25229.